

**Giant photoelasticity of polaritons for detection of coherent phonons
in a superlattice with quantum sensitivity**

Michal Kobecki,¹ Alexey V. Scherbakov,^{1,2} Serhii M. Kukhtaruk,^{1,3} Dmytro D. Yaremkevich,¹
Tobias Henksmeier,⁴ Alexander Trapp,⁴ Dirk Reuter,⁴ Vitaly E. Gusev,⁵ Andrey V. Akimov,⁶
and Manfred Bayer^{1,2}

¹*Experimentelle Physik 2, Technische Universität Dortmund, D-44227 Dortmund, Germany*

²*Ioffe Institute, Russian Academy of Sciences, 194021 St. Petersburg, Russia*

³*Department of Theoretical Physics, V.E. Lashkaryov Institute of Semiconductor Physics, 03028
Kyiv, Ukraine*

⁴*Department Physik, Universität Paderborn, 33098 Paderborn, Germany*

⁵*Laboratoire d'Acoustique de l'Université du Mans (LAUM), UMR 6613, Institut d'Acoustique -
Graduate School (IA-GS), CNRS, Le Mans Université, Le Mans, France*

⁶*School of Physics and Astronomy, University of Nottingham, Nottingham NG7 2RD, UK*

ABSTRACT

The functionality of phonon-based quantum devices largely depends on the efficiency of interaction of phonons with other excitations. For phonon frequencies above 20 GHz, generation and detection of phonon quanta can be monitored through photons. The photon-phonon interaction can be enormously strengthened by involving an intermediate resonant quasiparticle, e.g. an exciton, with which a photon forms a polariton. In this work, we discover giant photoelasticity of exciton-polaritons in a short-period superlattice and exploit it for counting propagating acoustic phonons. We demonstrate that 42 GHz coherent phonons can be detected with extremely high sensitivity in the time domain Brillouin oscillations by probing with photons in the spectral vicinity of the polariton resonance.

Recently coherent acoustic phonons with frequencies much higher than 1 GHz have shown their prospective in quantum technologies and nanophononics [1–6] due to their small wavelength which is comparable to the size of quantum nanodevices. Single localized phonon quanta are generated and detected using suspended nanostructures [1, 7–12] and propagating coherent phonons are suggested to become a logistic element in quantum computer networks [13–16]. Coherent phonons with frequency higher than 20 GHz can be excited and detected exclusively using optical techniques exploiting the photon-phonon interaction which governs the conversion of phonon to photon. Vice versa, its strength is the key factor determining the efficiency and energy consumption for optical interconversion into coherent phonons. There are already significant achievements in the efficient generation and detection of localized coherent phonons using non-suspended optomechanical nanoresonators [17–22]. However, for propagating phonons the sensitivity of optical methods has remained far from being able to count phonon quanta. The strength of photon-phonon coupling may be increased in non-cavity nanostructures hosting polariton resonances in which the photoelasticity increases drastically. An example is the exciton-polariton resonance in a short period semiconductor superlattice (SL) [23]. Recent experimental and theoretical studies of Brillouin scattering on thermal (i.e. noncoherent) phonons in the vicinity of a polariton resonance [24, 25] have indicated the potential ultra-sensitive detection of coherent phonons propagating in a SL.

In the present letter, we present the results of picosecond pump-probe experiments, in which we exploit an exciton-polariton resonance for detection of propagating coherent phonons with frequencies of ~ 42 GHz. The coherent phonon wavepacket propagating through a short-period SL is probed by measuring the reflectivity of picosecond optical pulses with photon energy in the vicinity of the polariton resonance. The measurements show that polaritons possess giant photoelasticity and provide a three orders of magnitude higher sensitivity for detection of propagating coherent phonons than when probing apart from the polariton resonance. We show that the giant sensitivity of optical reflection to phonon associated dynamical strain owned by the polariton resonance is sufficient for counting single phonon quanta in pump-probe setups.

The scheme of the experiment is presented in Fig.1(a). The studied SL grown by MBE on a 100- μm thick semi-insulating GaAs substrate consists of 30 periods of GaAs and AlAs layers with thicknesses of 12 and 14.2 nm, respectively. The background-free reflectivity spectrum $R_0(\hbar\omega)$ [see solid line in Fig. 1(b)] clearly shows the polariton resonance centered at $\hbar\omega_0 = 1.55$ eV. A wavepacket of coherent acoustic phonons is generated using pulsed optical excitation of the Al film with a thickness of 100 nm deposited on the substrate backside. The film is excited by the optical pump

pulses from a RegA laser system (wavelength 800 nm, pulse duration 200 fs, repetition rate 100 kHz) focused to a spot with diameter of 55 μm . The optically heated Al film expands and a coherent phonon wavepacket in form of a bipolar strain pulse with ~ 10 ps duration and amplitude η_0 is injected into the GaAs substrate [26, 27]. The typical simulated spatial profile for the used experimental scheme and materials [28], is shown in Fig. 1(c). The strain pulse, $\eta(t,z)$, propagates through the GaAs substrate with the velocity of longitudinal sound $v \approx 4800$ m/s, containing a broad spectrum of coherent longitudinal acoustic (LA) phonons with a maximum at frequency $f \sim 20$ GHz. The experiments are performed at temperature $T = 5$ K and phonons generated in the Al film reach the SL without attenuation. The coherent phonons are detected in the SL by measuring the reflectivity changes $\Delta R(t)$ of an optical probe pulse originating from the same laser.

First, we present $\Delta R(t)$ measured by the probe pulse taken straightforward from the laser system. The laser pulse with duration $\tau_{\text{pr}} = 200$ fs has the spectral width of 20 meV, which covers completely the spectrum around the polariton resonance. The detected transient signal is shown in Fig. 1(d). It possesses the oscillatory behavior that is known from time domain Brillouin scattering (TDBS) [29–31]. The time interval $-150 \leq t \leq 150$ ps, where the oscillations have a large amplitude, corresponds to the range when coherent phonons propagate through the SL toward the free surface, and after reflection at $t = 0$ ps in the opposite direction towards the substrate. The fast Fourier transform (FFT) of $\Delta R(t)$ shown in the lower panel of Fig. 1(e) demonstrates an intense line at $f_{\text{B}} = 42$ GHz and low intensity spectral lines with frequencies up to 450 GHz. The FFT spectrum agrees with the selection rule for TDBS $q = 2k_1$ (q and k_1 are the phonon and photon wave vectors in the SL, respectively) for normal incidence. The corresponding compliance is demonstrated in Fig. 1(e), where the upper panel shows the folded dispersion relations in the studied SL [32]. The TDBS signal in our SL is governed by propagating phonons which frequencies are far from the SL stop bands and phonon localization effects in the SL will not be considered further.

To study the effect of the SL polariton resonance on the TDBS signal we extend the duration of the probe pulse up to $\tau_{\text{pr}} = 1.35$ ps with a corresponding narrowing of its spectral width down to 1.4 meV by using a tunable LCD filter and measure the TDBS signal $\Delta R(t)$ for different central photon energy $\hbar\omega$. The spectrum of the extended probe pulse for $\hbar\omega = \hbar\omega_0$ is shown in Fig. 1(b) by the dashed red line. The value of $\hbar\omega$ is varied in the vicinity of the polariton resonance between 1.544 and 1.556 eV. In order to avoid nonlinear exciton effects [33, 34], we keep the probe fluence on the surface with the SL to less than 300 nJ/cm². Figure 2(a) shows the detected signal for a number of detuning

values $\hbar\omega - \hbar\omega_0$. It is seen that the amplitude of the oscillations strongly depends on the probe pulse photon energy.

Within the time interval when coherent phonons propagate in the SL, the measured signal can be fit with high precision by rising ($t < 0$) and decaying ($t > 0$) harmonic oscillations of single frequency, f_B , amplitude, A_B , phase, p_B , and recovery or decay rates, τ_B^{-1} , respectively. The dependences of these parameters are presented by the symbols in Figs. 2(b) and 2(c): open symbols for phonons propagating toward the free surface (anti-Stokes) and filled symbols for phonons propagating in the opposite direction after reflection (Stokes). The dependences are symmetric for A_B and τ_B^{-1} and antisymmetric for f_B and p_B relatively to $\hbar\omega_0$. This leads us to the conclusion that the TDBS signals and dependences A_B , τ_B^{-1} , f_B and p_B are governed by the polariton resonance when probing with $\hbar\omega$ close to $\hbar\omega_0$.

The exciting experimental result is the observation of the huge amplitude of the TDBS signal. When probing coherent phonons at the polariton resonance ($\hbar\omega = \hbar\omega_0$), the relative changes $\Delta R/R_0 \sim 10^{-2}$ for the used pump fluence $J \sim 0.1$ mJ/cm². The measurements of TDBS in materials without resonances for a similar wavepacket of coherent phonons would give $\Delta R/R_0 \sim 10^{-5}$ [32, 35] which is three orders of magnitude smaller than measured for the detection at the polariton resonance in the present work. This result means that our experiments reveal a giant photoelasticity of polaritons and extremely high sensitivity to propagating coherent Brillouin phonons.

With the assumption that the spectral width of the probe pulse is much smaller than the width of the polariton resonance, the amplitude of the TDBS signal can be estimated from the following equation [36]:

$$\frac{\Delta R(t)}{R_0} = 2\text{Re} \left[i \frac{1-r_{01}^2}{r_{01}} \frac{dk_1}{d\eta} \int_0^\infty \eta(z, t) e^{2ik_1 z} dz \right] \quad (1)$$

where $k_1 = 2\pi\tilde{n}/\lambda$ and \tilde{n} and λ are the complex refractive index in the SL and the wavelength of the probe light in vacuum, respectively, $r_{01} = (1 - \tilde{n})/(1 + \tilde{n})$ and $\eta(z, t) = \eta(z \pm vt)$ is the time-spatial profile of the strain pulse propagating along z in the SL toward the free surface (+) and backwards (-). The crucial parameter in Eq. (1) which governs the sensitivity of detection is the derivative of k_1 on strain η which is defined by the strain dependence of the effective dielectric function in the SL with the polariton resonance given by [37]:

$$\varepsilon_{\text{eff}}(\omega) = \varepsilon_b \left[1 + \frac{\omega_{\text{LT}}}{\omega_0 - \omega - i\Gamma} \right] \quad (2)$$

where ε_b is the background dielectric constant, ω_{LT} and Γ are the longitudinal-transverse splitting defined by the interaction of the excitons with light and the nonradiative decay rate of the polaritons.

The deformation potential mechanism is the main one responsible for the phonon-induced changes $\varepsilon_{\text{eff}}(\omega)$: the strain associated with coherent phonons induces the energy shift of the polariton resonance [38]. For a small number of phonons when this shift is much smaller than Γ we get

$$\frac{dk_1}{d\eta} = \frac{1}{2} \frac{k_1}{\varepsilon_{\text{eff}}} \frac{\Xi}{\hbar} \frac{d\varepsilon_{\text{eff}}}{d\omega_0} \quad (3)$$

where $\Xi = -10$ eV is the deformation potential for excitons in GaAs [39].

The presented model explains qualitatively the measured TDBS signals and dependences presented in Fig. 2(b) and 2(c). The explanation comes from the dependences of the real (n) and imaginary (κ) parts of the refractive index $\tilde{n} = \sqrt{\varepsilon_{\text{eff}}}$ and their derivatives on strain. They are shown in Figs. 2(d) and 2(e) for the polariton parameters, which fit our experimental data: $\hbar\omega_0 = 1.550$ eV, $\omega_{\text{LT}} = 0.13$ meV and $\Gamma = 0.7$ meV. It is seen that at $\hbar\omega = \hbar\omega_0 = 1.55$ eV $\left| \frac{dn}{d\eta} \right| \approx 4 \times 10^3$ possesses an extremum which results in the maximum for $A_{\text{B}}(\hbar\omega)$ [Fig. 2(b)]. Detuning $\hbar\omega$ away from the polariton resonance leads to the decreases of $\left| \frac{dn}{d\eta} \right|$ which obviously leads to the decrease of the TDBS signal amplitude observed experimentally. The dependence of f_{B} in Fig. 2(c) qualitatively follows $n(\hbar\omega)$, in full agreement with the wavevector selection rule $q = 2k_1$ for the phonon-polariton interaction which governs the TDBS signal. The measured dependence of the rising/decay rate τ_{B}^{-1} of the TDBS oscillations shown in the lower inset in Fig. 2(c) is similar to the dependence $\kappa(\hbar\omega)$, and the phase of the oscillations p_{B} changes by π in the vicinity of the polariton resonance [the upper inset in Fig. 2(c)], following the sign of $d\kappa/d\omega$.

The number of phonons, N_{B} , responsible for TDBS is determined by their spectral density \tilde{N} in the phonon wavepacket around the Brillouin frequency f_{B} . It is set by the integral in Eq. (1) and correspondingly determined by the spatial-temporal shape of the generated phonon wavepacket $\eta(z, t)$. Figure 2(f) is an example of the phonon spectral density for the strain pulse shown in Fig.1(c) with the amplitude $\eta_0 = 3 \times 10^{-5}$, which corresponds to $J = 0.5$ mJ/cm² [35]. The shaded area centered at the frequency $f_{\text{B}} = 42$ GHz indicates the spectral range of phonons detected at $\hbar\omega = \hbar\omega_0$. For a finite spectral width of 2 GHz, which is due to the finite penetration depth of light and the size of the SL, we obtain the density of detected phonons $N_{\text{B}} \approx 5 \times 10^3 \mu\text{m}^{-2}$.

For a quantitative analysis, we developed a comprehensive theoretical approach, which takes into account the spectral width of the probe pulse and the Stokes/anti-Stokes energy shift of the reflected light [40]. The solid curves in Figs. 2(b) and 2(c) are the results of calculations for the parameters given above. Excellent agreement between the measured and calculated dependences is

senn. The experimental and calculated sensitivities provide the signal amplitude $A_B = 3 \times 10^{-2}$ for $N = 5 \times 10^3 \mu\text{m}^{-2}$, which shows that the exciton-polariton phonon detector is a promising method for counting single phonon quanta. Indeed, if phonons with frequency f_B are emitted by a micrometer size semiconductor device [41], one SL phonon quantum in the probe spot of comparable size will induce a signal with amplitude exceeding 10^{-6} which can be reliably detected with high repetition rate pump-probe setups.

The experimental results and theoretical consideration presented above concern a small number of coherent phonons when the phonon-induced shift of the exciton resonances in the SL quantum wells is negligibly small. In this regime, the amplitude A_B of the TDBS oscillations depends linearly on the number of Brillouin phonons and, thus, linearly on J . This consideration should be not valid for high pump fluence when the maximum strain η_0 in the coherent phonon wavepacket induces the exciton shift $\Delta\hbar\omega_0 = \eta_0\Xi$ by a value comparable to the width Γ of the polariton resonance, the derivative of the dielectric function given by Eq. (3) becomes dependent on time and z . Qualitatively, at high J the polariton resonance broadens and at $\hbar\omega = \hbar\omega_0$ the sensitivity to Brillouin phonons decreases. Indeed, the dependence $A_B(J)$ measured at $\hbar\omega = \hbar\omega_0$ and shown in Fig. 3(a) by the symbols saturates at $J \approx 2 \text{ mJ/cm}^2$, and a further increase of J results in a decrease of A_B . The measured dependence perfectly agrees with the theoretical simulations [solid line in Fig. 3(a)] for the strain pulse shape shown in Fig.1(c) [40]. We have checked that the observed nonlinearity is not related to nonlinear acoustic effects [42, 43] which start to become pronounced in our experiment at $J > 3 \text{ mJ/cm}^2$.

Nonlinear photoelastic effects of the polaritons emerge also in the experimental and theoretical dependences $A_B(\hbar\omega)$ for high J as shown in Figs. 3(b) and 3(c). It is seen that at moderate $J = 2 \text{ mJ/cm}^2$, the experimentally measured spectral shape of $A_B(\hbar\omega)$ shifts by 1 meV relative to $\hbar\omega_0$. As can be seen in the middle and upper curves in Fig.3(a), blue and red shifts are measured for phonons propagating toward the free surface (anti-Stokes) and toward the substrate (Stokes), respectively. From this result, we may conclude that the incoming phonon wavepacket is asymmetric with a predominant compression component [28]. In contrary to the experimental results, the theoretical simulations show a spectral splitting of the dependence A_B on the probe photon energy, which is independent on the phonon propagation direction. This is explained by the bipolar symmetric strain pulse [see Fig.1(c)] used in the simulations. We have checked that a simulation with a unipolar compressive (tensile) strain pulse results in a blue (red) shift of $A_B(\hbar\omega)$.

In conclusion, we have demonstrated the effect of giant polariton photoelasticity for detecting propagating coherent phonon wavepackets by time domain Brillouin scattering. Our results pave a path for prospective exploitation of resonant polariton excitations for manipulating on the phonon quantum level. A strong dispersion of the permittivity in the visible range in the vicinity of the polariton resonance results in a huge ultrafast response of the optical properties to dynamical strain which accompanies the coherent phonons. We develop a quantitative theoretical model which allows us to predict the absolute values for the optical reflectivity change from propagating Brillouin phonons. The demonstrated that nonlinear effects for a boosted density of phonon flux suppress the sensitivity, in full agreement with the deformation potential model for exciton-phonon interactions used in treating the observed phenomena. The results show that polaritons have great prospective in counting single high-frequency phonon quanta.

Acknowledgements

We are grateful to Ilya Akimov, Nikolay Gippius, Mark Aßmann and Christine Silberhorn for fruitful discussions. The work was supported by the Deutsche Forschungsgemeinschaft (Grant No. TRR 142 project A06 and Grant No. TRR160 project A01).

References

- [1] K. J. Satzinger, Y. P. Zhong, H.-S. Chang, G. A. Peairs, A. Bienfait, M.-H. Chou, A. Y. Cleland, C. R. Conner, E' Dumur, J. Grebel, I. Gutierrez, B. H. November, R. G. Povey, S. J. Whiteley, D. D. Awschalom, D. I. Schuster, and A. N. Cleland, *Nature* **563**, 661 (2018).
- [2] S. Volz, J. Ordonez-Miranda, A. Shchepetov, M. Prunnila, J. Ahopelto, T. Pezeril, G. Vaudel, V. Gusev, P. Ruello, E. M. Weig et al., *Eur. Phys. J. B* **89**, 15 (2016).
- [3] W. H. Renninger, P. Kharel, R. O. Behunin, and P. T. Rakich, *Nat. Phys.* **14**, 601 (2018).
- [4] C. T. Hann, C.-L. Zou, Y. Zhang, Y. Chu, R. J. Schoelkopf, S. M. Girvin, and L. Jiang, *Phys. Rev. Lett.* **123**, 250501 (2019).
- [5] P. Delsing, A. N. Cleland, M. J. A. Schuetz, J. Knörzer, G. Giedke, J. I. Cirac, K Srinivasan, M. Wu, K. C. Balram, C Bäuerle et al., *J. Phys. D: Appl. Phys.* **52**, 353001 (2019).
- [6] A. A. Clerk, K. W. Lehnert, P. Bertet, and J. R. Petta, Y. Nakamura, *Nature Phys.* **16**, 257 (2020).
- [7] A. D. O'Connell, M. Hofheinz, M. Ansmann, Radoslaw C. Bialczak, M. Lenander, Erik Lucero, M. Neeley, D. Sank, H. Wang, M. Weides, J. Wenner, J. M. Martinis, A. N. Cleland, *Nature* **464**, 697 (2010).

- [8] J. D. Cohen, S. M. Meenehan, G. S. MacCabe, S. Gröblacher, A. H. Safavi-Naeini, F. Marsili, M. D. Shaw, and O. Painter, *Nature* **520**,522 (2015).
- [9] A. Noguchi, R. Yamazaki, Y. Tabuchi, and Y. Nakamura, *Phys. Rev. Lett.* **119**, 180505 (2017).
- [10] Y. Chu, P. Kharel, T. Yoon, L. Frunzio, P. T. Rakich, and R. J. Schoelkopf, *Nature* **563**, 666 (2018).
- [11] L. R. Sletten, B. A. Moores, J. J. Viennot, and K. W. Lehnert, *Phys. Rev. X* **9**, 021056 (2019).
- [12] G.ENZIAN, J. J. Price, L. Freisem, J. Nunn, J. Janousek, B. C. Buchler, P. K. Lam, and M. R. Vanner, *Phys. Rev. Lett.* **126**, 033601 (2021).
- [13] M. V. Gustafsson, T. Aref, A. F. Kockum, M. K. Ekstrom, G. Johansson, and P. Delsing, *Science* **346**, 207 (2014).
- [14] M. J. A. Schuetz, E. M. Kessler, G. Giedke, L. M. K. Vandersypen, M. D. Lukin, and J. I. Cirac, *Phys. Rev. X* **5**, 031031 (2015).
- [15] M.-A. Lemonde, S. Meesala, A. Sipahigil, M. J. A. Schuetz, M. D. Lukin, M. Loncar, P. Rabl, *Phys. Rev. Lett* **120**, 213603 (2018).
- [16] A. Bienfait, K. J. Satzinger, Y. P. Zhong, H.-S. Chang, M.-H. Chou, C. R. Conner, E. Dumur, J. Grebel, G. A. Peairs, R. G. Povey, and A. N. Cleland, *Science* **364**, 368 (2019).
- [17] W. Chen, Y. Lu, H. J. Maris, G. Xiao, *Phys. Rev. B* **50**, 14506 (1994).
- [18] A. Bartels, T. Dekorsy, and H. Kurz, *Phys. Rev. Lett.* **82**, 1044 (1999).
- [19] Huynh, N. D. Lanzillotti-Kimura, B. Jusserand, B. Perrin, A. Fainstein, M. F. Pascual-Winter, E. Peronne, and A. Lemaître, *Phys. Rev. Lett.* **97**, 115502 (2006).
- [20] N. D. Lanzillotti-Kimura, A. Fainstein, A. Huynh, B. Perrin, B. Jusserand, A. Miard, and A. Lemaître, *Phys. Rev. Lett.* **99**, 217405 (2007).
- [21] A. Fainstein, N. D. Lanzillotti-Kimura, B. Jusserand, and B. Perrin, *Phys. Rev. Lett.* **110**, 037403 (2013).
- [22] S. Anguiano, A. E. Bruchhausen, B. Jusserand, I. Favero, F. R. Lamberti, L. Lanco, I. Sagnes, A. Lematre, N. D. Lanzillotti-Kimura, P. Senellart, and A. Fainstein, *Phys. Rev. Lett.* **118**, 263901 (2017).
- [23] E. L. Ivchenko and G. E. Pikus, *Superlattices and other heterostructures, symmetry and optical phenomena*. 2nd ed. (Springer, Berlin Heidelberg, 1997).
- [24] A. N. Poddubny, A. V. Poshakinskiy, B. Jusserand, and A. Lemaître, *Phys. Rev. B* **89**, 235313 (2014).

- [25] B Jusserand, A. N. Poddubny, A. V. Poshakinskiy, A. Fainstein, and A. Lemaître, *Phys. Rev. Lett.* **115**, 267402 (2015).
- [26] C. Thomsen, H. T. Grahn, H. J. Maris, J. Tauc, *Phys. Rev. B* **34**, 4129 (1986).
- [27] O. Matsuda, M. C. Larciprete, R. Li. Voti, O. B. Wright, *Ultrasonics* **56**, 3 (2015).
- [28] D. Moss, A. V. Akimov, R. P. Champion, M. Henini, C. T. Foxon, L. Eaves, A. J. Kent, and B. A. Glavin, *Phys. Rev. B* **83**, 245303 (2011).
- [29] C. Thomsen, H. T. Grahn, H. J. Maris, and J. Tauc, *Optics Commun.* **60**, 55 (1986).
- [30] H. Lin, R. Stoner, H. Maris and J. Tauc, *J. Appl. Phys.* **69**, 3816 (1991).
- [31] O. B. Wright, *J. Appl. Phys.* **71**, 1617 (1992).
- [32] A. Huynh, B. Perrin, N. D. Lanzillotti-Kimura, B. Jusserand, A. Fainstein, and A. Lemaître, *Phys. Rev. B* **78**, 233302 (2008).
- [33] J. Oudar, J. Dubard, F. Alexandre, D. Hulin, A. Migus, and A. Antonetti, *J.de Phys. Colloq.* **48**, C5-511 (1987).
- [34] G. R. Hayes, J. L. Staehli, U. Oesterle, B. Deveaud, R. T. Phillips, and C. Ciuti, *Phys. Rev. Lett.* **83**, 2837 (1999).
- [35] A. V. Scherbakov, M. Bombeck, J. V. Jäger, A. S. Salasyuk, T. L. Linnik, V. E. Gusev, D. R. Yakovlev, A. V. Akimov, and M. Bayer, *Opt. Express* **21**, 16473 (2013).
- [36] V. Gusev, *Acustica Acta Acustica* **82**, S37 (1996).
- [37] V. A. Kosobukin, *Sov. Phys. Solid State* **34**, 1662 (1992).
- [38] A. V. Akimov, A. V. Scherbakov, D. R. Yakovlev, C. T. Foxon, and M. Bayer, *Phys. Rev. Lett* **97**, 037401 (2006).
- [39] F. H. Pollak and M. Cardona, *Phys. Rev.* **172**, 816 (1968).
- [40] See Supplemental Material for a detailed derivation of the simplified model, an analysis of the dependence of the TDBS signal on the phonon wavepacket spatial-temporal shape, and for a comprehensive theoretical approach used for calculations.
- [41] K. Cai, Z.-W. Pan, R.-X. Wang, D. Ruan, Z.-Q. Yin, and G.-L Long, *Optics Lett.* **43**, 1163 (2018)
- [42] H.-Y. Hao and H. J. Maris, *Phys. Rev. B* **64**, 064302 (2001).
- [43] E. Peronne, Ni. Chuecos, L. Thevenard, and B. Perrin, *Phys. Rev. B* **95**, 064306 (2017).

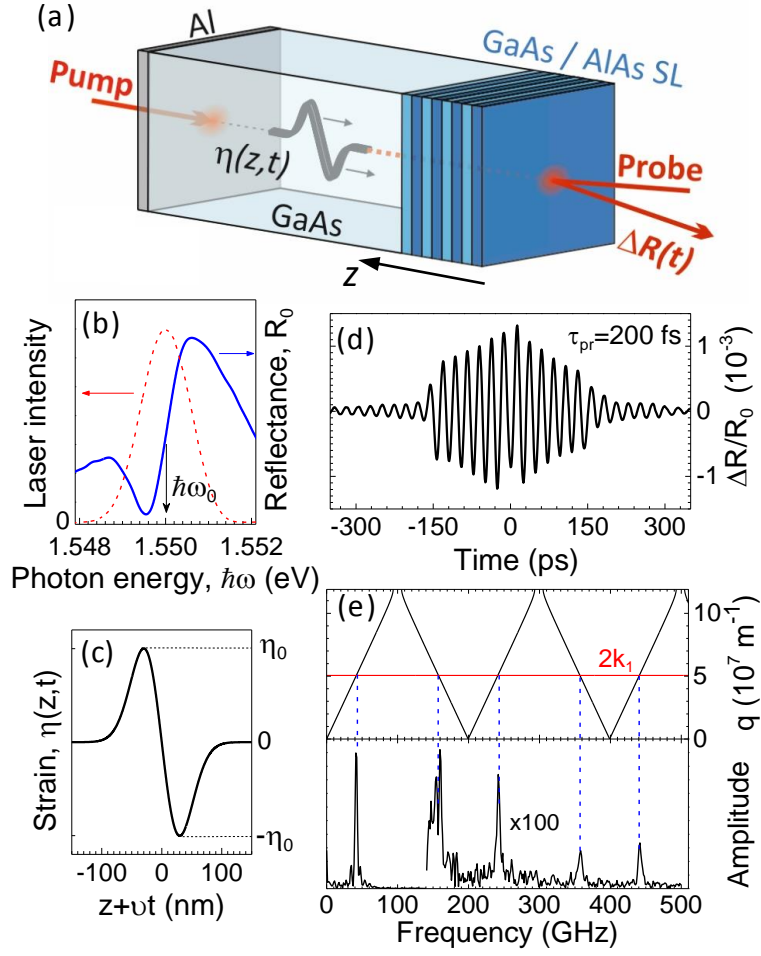


FIG. 1. (a) Experiment schematic. (b) Reflectivity spectrum in the vicinity of the polariton resonance (blue curve) with subtracted background. Dashed red curve shows the spectrum of the spectrally narrow probe pulse centered at the polariton resonance. (c) Simulated spatial profile of the strain pulse injected into the GaAs substrate from the Al phonon generator. (d) TDBS signal measured with probe pulses of 200-fs duration. Time $t = 0$ corresponds to the arrival of the phonon wavepacket center at the free surface of the SL. (e) Folded phonon dispersion of the studied superlattice (upper panel) and the fast Fourier transform of the transient reflectivity signal shown in (d) (lower panel).

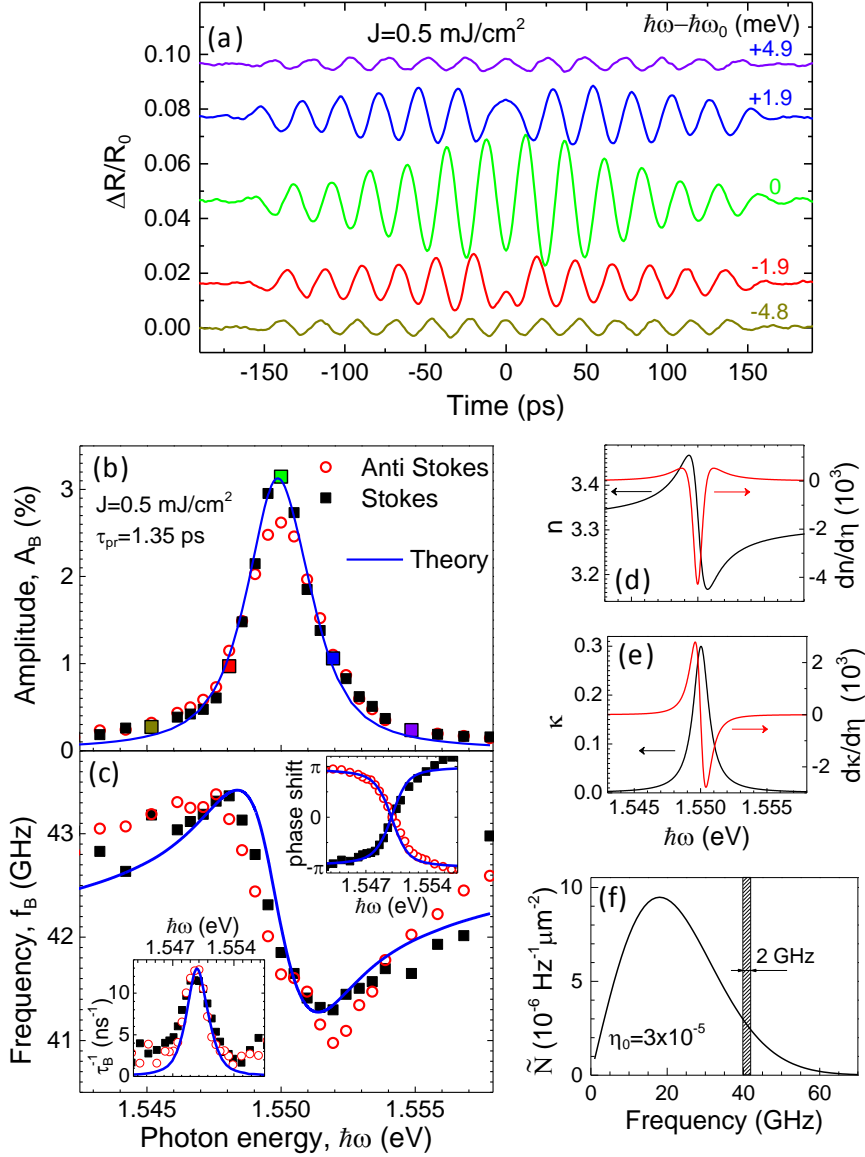


FIG. 2. (a) TDBS signals measured by the spectrally narrow probe pulses for several $\hbar\omega$. (b,c) Dependences of the specific properties of the TDBS signals on the probe photon energy: amplitude A_B (a), frequency f_B (b), decay rate τ_B^{-1} [lower insert in (c)], and shift of the phase p_B relative to the signal measured at resonant conditions [upper insert in (c)]. Enlarged colored symbols in (b) correspond to the transient signals shown by the same color in (a). (d,e) Calculated spectral dependences of the real and imaginary part of refractive index and their derivatives

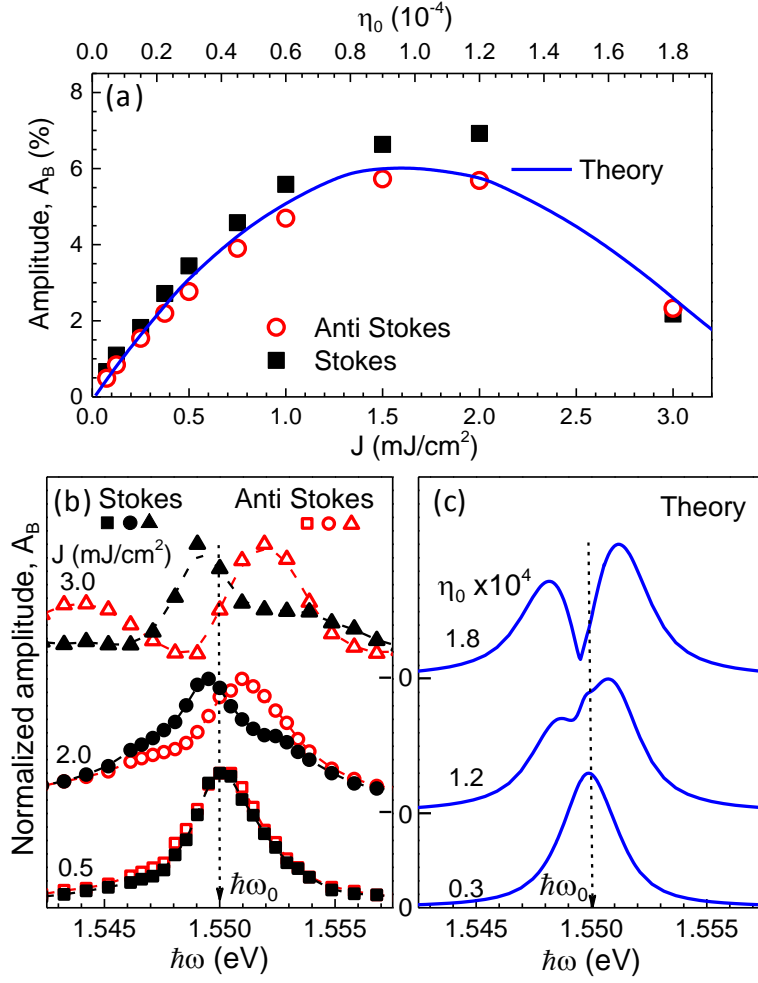


FIG. 3. (a) Dependence of the TDBS signal amplitude on the optical excitation density (experimental data, symbols) and the strain pulse amplitude (theoretical calculations, solid lines). (b,c) Measured (b) and calculated (c) dependences of the TDBS signal amplitude on the probe photon energy for three values of J and η_0 , respectively. The dependences are normalized to the values at the maxima.

Giant photoelasticity of polaritons for detection of coherent phonons in a superlattice with quantum sensitivity

Michal Kobecki,¹ Alexey V. Scherbakov,^{1,2} Serhii M. Kukhtaruk,^{1,3} Dmytro D. Yaremkevich,¹
Tobias Henksmeier,⁴ Alexander Trapp,⁴ Dirk Reuter,⁴ Vitaly E. Gusev,⁵ Andrey V. Akimov,⁶
and Manfred Bayer^{1,2}

¹*Experimentelle Physik 2, Technische Universität Dortmund, 44227 Dortmund, Germany*

²*Ioffe Institute, 194021 St. Petersburg, Russia*

³*Department of Theoretical Physics, V.E. Lashkaryov Institute, 03028 Kyiv, Ukraine*

⁴*Department Physik, Universität Paderborn, 33098 Paderborn, Germany*

⁵*Laboratoire d'Acoustique de l'Université du Mans (LAUM), UMR 6613, Institut d'Acoustique - Graduate School (IA-GS), CNRS, Le Mans Université, Le Mans, France*

⁶*School of Physics and Astronomy, University of Nottingham, Nottingham NG7 2RD, UK*

Supplemental material

This supplemental material includes two theoretical parts where the coherent phonon wavepacket is considered classically as dynamical strain dependent on the coordinate z and time t . The first part presents a theoretical model describing the scattering of the coherent laser pulses with very narrow spectrum by the polaritons, which are loaded by the dynamical strain. This analytical model provides a clear qualitative insight into the observed linear and nonlinear photo-elastic phenomena. The second part extends this model for the general case of arbitrary durations of coherent probe light and strain pulses. This consideration includes numerical calculations providing quantitative data of the strain induced changes in transient optical reflectivity for the comparison with experimental results.

1. Adiabatic response of exciton optical polarization to dynamical strain

Propagation of a plane electromagnetic wave along the z -axis (the coordinate system corresponds to the one used in the main text with z -axis normal to the surface) in a medium possessing the relative permittivity ϵ_b in presence of the excitons is described as

$$\frac{\partial^2 E}{\partial z^2} - \frac{\epsilon_b}{c_0^2} \frac{\partial^2 E}{\partial t^2} = \frac{1}{\epsilon_0 c_0^2} \frac{\partial^2 P}{\partial t^2}, \quad (1)$$

where E and P are the y -components of the electric field and the exciton polarization, respectively, ϵ_0 and c_0 are the permittivity and the light velocity in vacuum, and t is the time variable. The equation for the exciton polarization driven by light in the presence of the dynamical strain can be written in the form [1]:

$$\frac{\partial P}{\partial t} + i[\omega_0 + \epsilon(z, t) - i\Gamma]P = i\epsilon_0 \omega_p E, \quad (2)$$

where ω_0 and Γ are the exciton resonance frequency and the inverse lifetime (the latter accounts for the contributions of both radiative and non-radiative processes); the cyclic frequency ω_p characterizes the strength the exciton-photon coupling and $\epsilon(z, t)$ describes the strain-induced shift of the exciton resonance. This shift is $\epsilon(z, t) = \frac{\Xi}{\hbar} \eta(z, t)$, where Ξ is the deformation potential, \hbar the reduced Planck constant and $\eta(z, t)$ in the normal (longitudinal) strain. The solution of Eq. (2) reveals the following dynamics of the exciton in response to dynamical strain:

$$P = i\epsilon_0 \omega_p \int_{-\infty}^t dE(z, t') e^{-i[(\omega_0 - i\Gamma)(t-t') + \int_{t'}^t dt'' \epsilon(z, t'')]} \quad (3)$$

In the case of the monochromatic electromagnetic wave with frequency ω (the case of long probe laser pulses), described by $E(z, t) = E(z)e^{-i\omega t}$ the polarization field in Eq. (3) takes the form

$$P = i\varepsilon_0\omega_p E(z)e^{-i\omega t} \int_0^\infty d\tau e^{-i[(\omega_0 - \omega - i\Gamma)\tau + \int_{t-\tau}^t dt' \varepsilon(z, t')]} \quad (4)$$

describing the modulation of monochromatically varying polarization of the exciton by dynamical strain. Because the phonon frequencies are much lower than the optical one, the modulation is slow in time and the polarization of the exciton is quasi-monochromatic. Characteristic life/decay time of the exciton resonance, $\tau_\Gamma \equiv \frac{1}{\Gamma}$ in our experimental sample with $\hbar\Gamma \approx 0.7$ meV is $\tau_\Gamma \approx 1$ ps. In the linear acoustic regime, the duration of the photo-generated strain pulse τ_a is controlled by the longitudinal sound velocity and thickness of a metallic phonon generator and in our experiment, exceeds 10 ps. Thus, the inequality $\tau_\Gamma \ll \tau_a$ allows analytical integration of Eq. (4) for the arbitrary strain spatial profile in the adiabatic regime. The adiabatic response of the exciton polarization to the dynamical strain in this asymptotic case is

$$P = \varepsilon_0 \frac{\omega_p}{\omega_0 - \omega - i\Gamma + \varepsilon(z, t)} E(z) e^{-i\omega t}. \quad (5)$$

Then, the electromagnetic wave equation (1) is reduced to

$$\frac{\partial^2 E(z)}{\partial z^2} + \frac{\varepsilon_{\text{eff}} + \Delta\varepsilon(\eta)}{c_0^2} \omega^2 E(z) = 0. \quad (6)$$

Here ε_{eff} denotes permittivity of the medium with excitons:

$$\varepsilon_{\text{eff}} \equiv \varepsilon_b + \frac{\omega_p}{\omega_0 - \omega - i\Gamma}, \quad (7)$$

while $\Delta\varepsilon$ denotes the strain-induced modifications of permittivity:

$$\Delta\varepsilon(\eta) \equiv \varepsilon_b(\eta) - \varepsilon_b(\eta = 0) + \frac{\omega_p}{\omega_0 - \omega - i\Gamma + \varepsilon(z, t)} - \frac{\omega_p}{\omega_0 - \omega - i\Gamma} \equiv \Delta\varepsilon_b(\eta) - \frac{\omega_p \varepsilon(z, t)}{[\omega_0 - \omega - i\Gamma + \varepsilon(z, t)][\omega_0 - \omega - i\Gamma]}. \quad (8)$$

Equation (8) splits the contributions to the photo-elastic effect due to the background material, i.e. $\Delta\varepsilon_b(\eta)$, and due to the excitons. The prediction of the strain-induced modifications of the permittivity in Eq. (8) provides opportunity to adapt the classical theory for the strain-induced transient reflectivity changes in picosecond ultrasonic experiment [2,3] with minor modifications for the considered system. In the case of small strain $|\eta| \leq 10^{-3}$ and for the typical sensitivity of permittivity to the strain $|\partial\varepsilon/\partial\eta| \leq 10$ one may use a linearized description of $\Delta\varepsilon(\eta)$, i.e., $\Delta\varepsilon(\eta) \cong \partial\varepsilon/\partial\eta(\eta = 0)\eta$. In our experiment, however, this approximation holds for the description of the photo-elastic response of the background, but is not always valid for the contribution from the excitons due to their extremely high photoelasticity [1]. Thus, $\Delta\varepsilon(\eta) \cong \partial\varepsilon/\partial\eta(\eta = 0)\eta$ used in the conventional formalism should be replaced by

$$\Delta\varepsilon(\eta) \equiv \partial\varepsilon_b/\partial\eta(\eta = 0)\eta - \frac{\omega_p \varepsilon(z, t)}{[\omega_0 - \omega - i\Gamma + \varepsilon(z, t)][\omega_0 - \omega - i\Gamma]}. \quad (9)$$

For the considered experiment, we assume that the dominant contribution to the medium permittivity ε_{eff} is given by the background, i.e.,

$$\left| \frac{\omega_p}{\omega_0 - \omega - i\Gamma} \right| \ll |\varepsilon_b| \text{ or } \left| \frac{\omega_{\text{LT}}}{\omega_0 - \omega - i\Gamma} \right| \ll 1, \quad (10)$$

while in the spectral vicinity of the exciton resonance ω_0 the photoelastic response is determined by excitons:

$$\left| \frac{\partial\varepsilon_b}{\partial\eta} / \varepsilon_b(\eta = 0) \right| \ll \left| \frac{\omega_p \omega_d}{[\omega_0 - \omega - i\Gamma + \omega_d \eta(z, t)][\omega_0 - \omega - i\Gamma]} \right|, \quad (11)$$

where the cyclic frequency $\omega_d = \frac{\Xi}{\hbar}$ characterizes the magnitude of the exciton-phonon deformation potential. In Eq. (10) we assumed that $\omega_p \approx \varepsilon_b \omega_{\text{LT}}$, where ω_{LT} is the so-called longitudinal-transverse splitting (see e.g. [1]). For $\hbar\omega_{\text{LT}} \sim 0.13$ meV [1] in the spectral vicinity of the exciton resonance, $\omega \approx \omega_0$, $\frac{\omega_{\text{LT}}}{\Gamma} \approx 0.2$ and Eq. (10) is well

satisfied. The validity of Eq. (11), depends on the strain amplitude, because the dependence of the response of the exciton permittivity to the dynamical strain is not linearized yet. The structure of the denominator in the right-hand-side of Eq. (11) indicates that the linear regime in the photoelastic response of the exciton is determined by the condition $|\omega_d \eta(z, t)| = |\epsilon(z, t)| \ll \Gamma$, i.e., the linear regime takes place when the strain-induced shift of the exciton resonance is much less than its spectral width. For the typical values of the exciton-phonon deformation potential $\Xi \sim -10$ eV, the linear regime is expected for $|\eta(z, t)| \ll 7 \times 10^{-5} \sim 10^{-4}$. At larger strain the amplitude of the permittivity changes induced by dynamical strain saturates. This follows from the structure of the exciton contribution to the strain-induced permittivity changes in Eq. (9) (which are separately rewritten below in Eq. (12)) where both nominator and denominator are linear functions of the strain field magnitude. Thus, the amplitude of the strain-induced permittivity changes, $|\Delta\epsilon(\eta)|$, starts to be independent on the strain field there and then, where and when $|\omega_d \eta(z, t)| = |\epsilon(z, t)| \gg \max\{|\omega_0 - \omega|, \Gamma\}$.

We can estimate the validity of Eq. (11) in our experiment. At resonance for the parameters of the studied sample, it takes form

$$\left| \frac{\partial \epsilon_b}{\partial \eta(\eta=0)} / \epsilon_b(\eta = 0) \right| \ll \left| \frac{\omega_{LT} \omega_d}{\Gamma^2} \right| \approx 3 \times 10^3$$

For the probe pulse wavelengths around 800 nm at the experimental temperature of 5 K, $\epsilon_b = \epsilon_{GaAs} \approx 11$ and $\frac{\partial \epsilon_b}{\partial \eta}(\eta = 0, T = 5 \text{ K}) \leq \frac{\partial \epsilon_{GaAs}}{\partial \eta}(\eta = 0, T = 293 \text{ K}) \approx 18.2$ [5]. Thus, $\left| \frac{\partial \epsilon_b}{\partial \eta(\eta=0)} / \epsilon_b(\eta = 0) \right| \leq 2$. Therefore, it is confirmed by the estimates that the classical formulas for the strain-induced transient optical reflectivity signals [2,3] can be applied in our experiments with approximation of the background permittivity by $\epsilon_b \cong \epsilon_{GaAs}$ and the strain induced modifications of the permittivity by

$$\Delta\epsilon(\eta) \cong - \frac{\epsilon_b \omega_{LT} \omega_d \eta(z, t)}{[\omega_0 - \omega - i\Gamma + \omega_d \eta(z, t)][\omega_0 - \omega - i\Gamma]}. \quad (12)$$

The photoelastic parameter p , classically defined by the relation $p \equiv \frac{\partial(\frac{1}{\epsilon})}{\partial \eta}(\eta = 0) = -\frac{1}{\epsilon^2} \frac{\partial \epsilon}{\partial \eta}(\eta = 0)$, reaches its maximal value in the linear regime of exciton-phonon interaction. In our sample the estimated value of the linear photoelastic parameter in resonance of the exciton is $p = -\frac{1}{\epsilon_{GaAs}} \frac{\omega_{LT} \omega_d}{\Gamma^2} \cong -3 \cdot 10^2$, leading to giant sensitivity in the detection of coherent acoustic phonons via monitoring of the transient permittivity variations. It is worth noting, however, that estimated here photoelastic constant is more than 100 times smaller than one estimated in [4].

The complete description of the Brillouin oscillations in the transient reflectivity signals caused by the propagating strain pulse in an infinite short-period superlattice (SL) under above-stated conditions (10) and (11) in the adiabatic regime could be derived by substituting Eq. (12) in the following formula for the probe light transient reflectivity

$$\frac{\Delta R}{R_0} = Re \left[i \left(\frac{1-r_{01}^2}{r_{01}} \right) \frac{k_0^2}{k_1} \int_0^\infty dz \Delta\epsilon(\eta) e^{2ik_1 z} \right]. \quad (13)$$

In Eq. (13) r_{01} and $k_{0,1}$ denote the reflection coefficient for the electric field in transition from air into SL and the probe light wave numbers in air and SL, respectively. The optical parameters of the SL can be approximated by the parameters of the background material. The derivations of the formulas, similar or equivalent to Eq. (13) in similar or more complicated experimental geometries can be found in Refs. [2,3], for example. When in the solution (13) only the strain-induced permittivity changes are taken into account, the transient reflectivity described by Eq. (13) is called time-domain Brillouin scattering (TDBS) signal. This notation indicates the relation of the scattered light to the presence of strain perturbation in the medium, although the scattering is governed not directly by the strain, but by the permittivity changes

ressing the dynamical strain. Because GaAs is practically transparent for the probe light at 800 nm, the combination of Eqs. (12) and (13) leads to

$$\frac{dR}{R_0} = -\left(\frac{1-r_{01}^2}{r_{01}}\right) k_1 \text{Re} \left[i \frac{\omega_{LT}}{[\omega_0 - \omega - i\Gamma]} \int_0^\infty dz \frac{\omega_d \eta(z,t)}{[\omega_0 - \omega - i\Gamma + \omega_d \eta(z,t)]} e^{2ik_1 z} \right]. \quad (14)$$

Equation (14) predicts that in the general case, both the amplitude and the phase of the Brillouin oscillations depend on the spatial profile and amplitude of the strain pulse, $\eta(z, t)$. We present the analysis of several simple strain profiles, which allow an analytical evaluation of Eq. (14). For the sake of compactness, we limit our consideration here only by the case of the resonant optical excitation: $\omega = \omega_0$. The profile of the strain pulse propagating along the z axis is introduced via $\eta(z, t) = \eta_0 S\left(\frac{z-vt}{l_a}\right) = \eta_0 S\left(\frac{z-vt}{|v|\tau_a}\right) \equiv \eta_0 S(\xi)$, where v denotes the longitudinal sound velocity, the sign of v controls the direction of propagation and η_0 is the characteristic strain magnitude, which could be either positive or negative. Equation (14) can be consequently rewritten as

$$\begin{aligned} \frac{dR}{R} &= \left(\frac{1-r_{01}^2}{r_{01}}\right) k_1 \frac{\omega_{LT}}{\Gamma} \text{Re} \left[\int_0^\infty dz \frac{\eta(z,t)}{\eta(z,t) - i\frac{\Gamma}{\omega_d}} e^{2ik_1 z} \right] \equiv \\ &\left(\frac{1-r_{01}^2}{r_{01}}\right) k_1 \frac{\omega_{LT}}{\Gamma} v \tau_a \text{Re} \left[e^{i\omega_B t} \int_{\frac{|t|}{\tau_a}}^\infty d\xi \frac{S(\xi)}{S(\xi) - i\frac{\Gamma}{\eta_0 \omega_d}} e^{i\bar{k}_B \xi} \right]. \end{aligned} \quad (15)$$

Here, $\omega_B = 2k_1 v$ denotes the cyclic frequency of the Brillouin oscillation and compact notations for two non-dimensional parameters $\frac{\Gamma}{\eta_0 \omega_d} \equiv \bar{\Gamma} \equiv \frac{1}{\bar{\eta}_0}$ and $2k_1 l_a = |\omega_B| \tau_a \equiv \bar{k}_B$ are introduced. When $t \leq 0$ and $t \geq 0$ the solution in Eq. (14) is valid for the phonons propagating towards the mechanically free surface, i.e., < 0 , and from the mechanically free surface, i.e., > 0 , respectively. Under the condition $|t| \geq \tau_a$, i.e., when the launched strain pulse is completely inside the SL, the final solution for the description of the Brillouin oscillations revealed by Eq. (15) is presented in the form

$$\frac{dR}{R} \cong \left(\frac{1-r_{01}^2}{2r_{01}}\right) \frac{\omega_{LT}}{\Gamma} \bar{k}_B \cdot \text{Re} \left[e^{i\omega_B t} \int_{-\infty}^\infty d\xi \frac{S(\xi)}{S(\xi) - i\bar{\Gamma}} e^{i\bar{k}_B \xi} \right] \equiv A \cdot \text{Re} \left[e^{i\omega_B t} \int_{-\infty}^\infty d\xi \frac{i\bar{\eta}_0 S(\xi)}{1 + i\bar{\eta}_0 S(\xi)} e^{i\bar{k}_B \xi} \right]. \quad (16)$$

The solutions in Eqs. (15), (16) evidence that TDBS is selectively sensitive to a particular spatial spectrum component of the permittivity pulse which is dressing the dynamical strain. The particular detected component is one with the Brillouin wave number ($k_B = 2k_1$). It is equal to the wave number of the coherent acoustic phonons with the Brillouin frequency. Note that $\bar{\eta}_0$ is either positive or negative, depending on the signs of η_0 and of the deformation potential Ξ . The integration in Eq. (16) can be done analytically on the complex plane for several simple models of the strain profile.

For the unipolar Lorentzian dynamical strain profile $S(\xi) = \frac{1}{1+\xi^2}$, the result is

$$\frac{dR}{R} \cong -A\pi\bar{\eta}_0 \text{Re} \left[\frac{1}{\xi_p' + i\xi_p''} e^{i\bar{k}_B(\xi_p' + i\xi_p'')} e^{i\omega_B t} \right] = -A\pi \frac{\bar{\eta}_0}{|\xi_p|} e^{-\bar{k}_B \xi_p''} \cos \left[\omega_B t + \bar{k}_B \xi_p' - \arctan \left(\frac{\xi_p''}{\xi_p'} \right) \right]. \quad (17)$$

Here ξ_p denotes the coordinates of the contributing pole on the complex plane

$$\xi_p = \xi_p' + i\xi_p'' = \frac{1}{\sqrt{2}} \left[\sqrt{\sqrt{1 + \bar{\eta}_0^2} - 1} + i\sqrt{\sqrt{1 + \bar{\eta}_0^2} + 1} \right]. \quad (18)$$

The solution in Eqs. (17) and (18) predicts the following dependence of the amplitude of the Brillouin oscillation on the normalized strain amplitude $\bar{\eta}_0$

$$\left| \frac{dR}{R} \right| \sim \frac{|\bar{\eta}_0|}{\sqrt{1 + \bar{\eta}_0^2}} e^{-\bar{k}_B \frac{1}{\sqrt{2}} \sqrt{\sqrt{1 + \bar{\eta}_0^2} + 1}}, \quad (19)$$

which reveals the expected growth $\sim |\bar{\eta}_0|$ in the earlier defined linear regime ($|\omega_d \eta(z, t)| \ll \Gamma$, i. e., $|\bar{\eta}_0| \ll 1$) and an exponential decay $\sim e^{-\frac{1}{\sqrt{2}} \bar{k}_B \sqrt{|\bar{\eta}_0|}}$ in the strongly nonlinear regime ($|\bar{\eta}_0| \gg 1$). The strain magnitude η_0^{max} , for which the maximum in the amplitude of the Brillouin oscillations can be achieved, depends on the non-dimensional parameters \bar{k}_B

and $\frac{\Gamma}{\omega_d}$, through the following relation: $\bar{k}_B = \frac{2\sqrt{2} \sqrt{\sqrt{1+\eta_0^{max^2}}+1}}{\eta_0^{max^2} \sqrt{1+\eta_0^{max^2}}}$, plotted in Fig. 1 (a) in black lines. Note, that the structure

and the asymptotic behaviors in the case of unipolar strain profile is the same for the compression and tension pulses. Therefore, in Fig. 1(b) only one dependence of η_0^{max} on the duration of unipolar Lorentzian pulse τ_a is presented for our known experimental conditions, i. e., for Γ and Ξ already listed earlier, and Brillouin frequency about 42.5 GHz.

2) **Bipolar Lorentzian strain pulse:** $S(\xi) = \frac{2\xi}{1+\xi^2}$,

$$\frac{dR}{R_0} \cong -A2\pi \frac{\bar{\eta}_0 \left[\sqrt{1+\bar{\eta}_0^2} - \bar{\eta}_0 \right]}{\sqrt{1+\bar{\eta}_0^2}} e^{-\bar{k}_B \left[\sqrt{1+\bar{\eta}_0^2} - \bar{\eta}_0 \right]} \cos[\omega_B t], \quad \left| \frac{dR}{R} \right| \sim \frac{|\bar{\eta}_0| \left[\sqrt{1+\bar{\eta}_0^2} - \bar{\eta}_0 \right]}{\sqrt{1+\bar{\eta}_0^2}} e^{-\bar{k}_B \left[\sqrt{1+\bar{\eta}_0^2} - \bar{\eta}_0 \right]}. \quad (20)$$

The behaviors predicted in Eq. (20) for bipolar pulses are different from those of unipolar pulses. They also importantly depend on the sign of $\bar{\eta}_0$. When $\bar{\eta}_0 > 0$, the amplitude of the Brillouin oscillation is $\sim \bar{\eta}_0$ in the linear regime ($\bar{\eta}_0 \ll 1$), but decreases non-exponentially $\sim \frac{1}{\bar{\eta}_0} e^{-\frac{\bar{k}_B}{2\bar{\eta}_0}}$ in the strongly nonlinear regime ($\bar{\eta}_0 \gg 1$). The latter asymptotic shows the diminishing of the Brillouin oscillation amplitude only if the condition $\bar{\eta}_0 > \bar{k}_B/2$ is satisfied simultaneously with $\bar{\eta}_0 \gg 1$. When $\bar{\eta}_0 < 0$, the amplitude of the Brillouin oscillation is $\sim |\bar{\eta}_0|$ in the linear regime ($|\bar{\eta}_0| \ll 1$), but decreases non-exponentially $\sim |\bar{\eta}_0| e^{-2\bar{k}_B |\bar{\eta}_0|}$ in the strongly nonlinear regime ($|\bar{\eta}_0| \gg 1$). In both cases, the decay of the Brillouin oscillation amplitude in strongly nonlinear regime is slower in the case of bipolar pulses in comparison with the unipolar pulses of the same amplitude.

The phonon-induced strain magnitude η_0^{max} , for which the maximum in the amplitude of the Brillouin oscillations can be achieved, depends also on the dimensionless parameters \bar{k}_B and $\frac{\Gamma}{\omega_d}$, but through an alternate relation:

$$\bar{k}_B = \frac{1 - \frac{1}{\eta_0^{max} \sqrt{1+(\eta_0^{max})^2}}}{\sqrt{1+(\eta_0^{max})^2} - \eta_0^{max}}, \quad (21)$$

which gives the dependences shown in Fig. 1 (a) by the red lines. For $f_B = 42.5$ GHz and the strain pulse duration $\tau_a = 12.5$ ps, the theoretical prediction is $\eta_0^{max} \approx 2 \cdot 10^{-5}$ as evidenced by Fig. 1 (b). This value is about 5 times smaller than the experimental one (see Fig. 3 (a) of the main manuscript) because the description of the strain profile based on Lorentzian function is much less adequate for our experiments than one based on Gaussian function. Numerical fits in the main manuscript were based on the generalized theory presented in the second part of the Supplemental materials, which used the first derivative of the Gaussian function for the profile of a bipolar strain pulse. It can be appreciated in Fig. 3 (a) that with the same fitting parameters, the assumption of the Gaussian strain profile reproduces the experimental η_0^{max} much better than the assumption of the Lorentzian strain profile. From the physics point of view, for the equal characteristic lengths, the Gaussian profiles are significantly better localized than the Lorentzian ones in terms of the

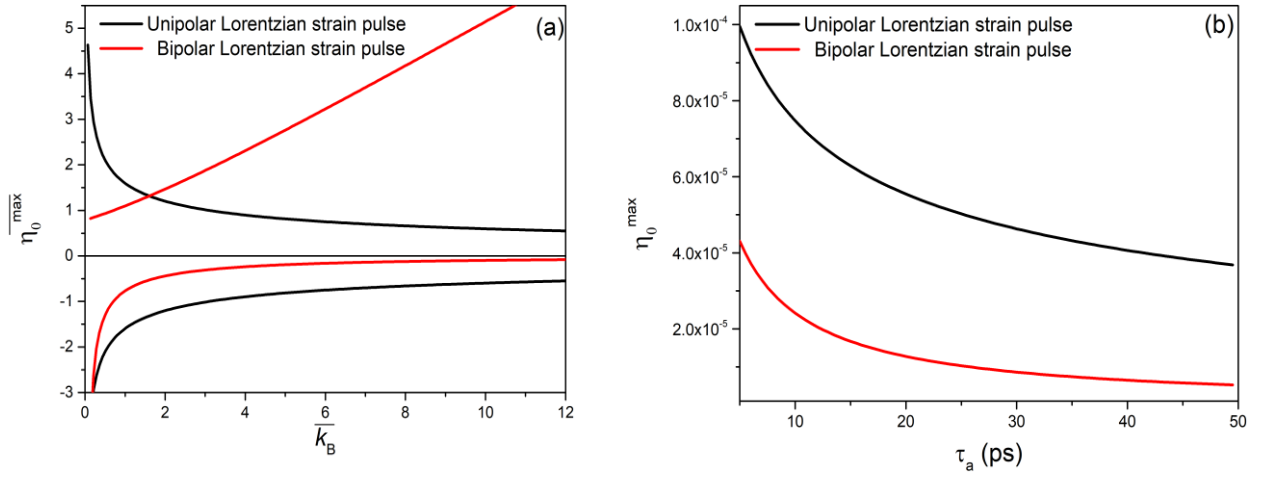


Figure 1. (a) Dependences of the normalized strain magnitude $\bar{\eta}_0^{\max}$ of the Lorentzian strain profile required for reaching the maximum of the Brillouin oscillation amplitude on the normalized Brillouin wave number. The deformation potential in $\bar{\eta}_0^{\max}$ could be either positive or negative. (b) Dependences of the strain magnitude η_0^{\max} required for reaching the maximum of the Brillouin oscillations amplitude on the durations of unipolar and bipolar Lorentzian strain pulses, under the conditions of our experiments. The leading phase of the bipolar pulse incident on the mechanically free surface of the SL is compression (corresponding to $\eta_0 > 0$ for the strain profile $S(\xi) = 2\xi/(1 + \xi^2)$), while the deformation potential is negative. Black and red lines are for the unipolar and bipolar strain profile, respectively.

decay of the wings at increasing distances from the wavepacket center. As it would be confirmed below, this leads to significantly slower development of the nonlinear photo-elastic processes in the case of Gaussian CWP than in the case of Laurentzian CPW.

To clarify qualitatively the differences in the monitoring by TDBS of the unipolar and bipolar strain pulses, it is instructive to split the real and imaginary parts of strain dependent part of $\Delta\varepsilon$ in Eq. (15):

$$\left| \frac{dR}{R} \right| \sim \left| \int_{-\infty}^{\infty} d\xi \frac{i\bar{\eta}_0 S(\xi)}{1+i\bar{\eta}_0 S(\xi)} e^{i\bar{k}_B \xi} \right| = \left| \int_{-\infty}^{\infty} d\xi \left[\frac{\bar{\eta}_0^2 S^2(\xi)}{1+\bar{\eta}_0^2 S^2(\xi)} + i \frac{\bar{\eta}_0 S(\xi)}{1+\bar{\eta}_0^2 S^2(\xi)} \right] e^{i\bar{k}_B \xi} \right| \quad (22)$$

The subsequent transformation of this formula differs for the symmetric (even) unipolar pulses, satisfying the condition $S(-\xi) = S(\xi)$, and anti-symmetric (odd) bipolar pulses, satisfying the condition $S(-\xi) = -S(\xi)$.

For the defined above unipolar pulses:

$$\left| \frac{dR}{R} \right| \sim \left| \int_{-\infty}^{\infty} d\xi \left[\frac{\bar{\eta}_0^2 S^2(\xi)}{1+\bar{\eta}_0^2 S^2(\xi)} + i \frac{\bar{\eta}_0 S(\xi)}{1+\bar{\eta}_0^2 S^2(\xi)} \right] \cos(\bar{k}_B \xi) \right|, \quad (23)$$

and, consequently, $\left| \frac{dR}{R} \right|$ depends only on $\bar{\eta}_0^2$ and does not depend on the sign of $\bar{\eta}_0$.

For the above defined bipolar pulse the final result is different because both real and imaginary parts of $\Delta\varepsilon$ provide real contribution to the \bar{k}_B component of the spatial Fourier spectrum of $\Delta\varepsilon$:

$$\left| \frac{dR}{R} \right| \sim \left| \int_0^{\infty} d\xi \left[\frac{\bar{\eta}_0^2 S^2(\xi)}{1+\bar{\eta}_0^2 S^2(\xi)} \cos(\bar{k}_B \xi) - \frac{\bar{\eta}_0 S(\xi)}{1+\bar{\eta}_0^2 S^2(\xi)} \sin(\bar{k}_B \xi) \right] \right|. \quad (24)$$

This formula provides evidence on the dependence of the Brillouin oscillation amplitude on the polarity of the bipolar pulse. However, the dependence on sign of $\bar{\eta}_0$ manifests itself only in the nonlinear regime, when the contribution of the Real part of $\Delta\varepsilon$ becomes not too small in comparison with the contribution from the imaginary part of $\Delta\varepsilon$.

In the linear regime $\bar{\eta}_0 \ll 1$

$$\left| \frac{dR}{R} \right| \sim |\bar{\eta}_0| \left| \int_0^{\infty} d\xi S(\xi) \sin(\bar{k}_B \xi) \right|. \quad (25)$$

For the general case of an arbitrary $\overline{\eta}_0$ it is instructive to rewrite the solution for the symmetric bipolar pulse as

$$\left| \frac{dR}{R} \right| \sim |\overline{\eta}_0| \left| \int_0^\infty d\xi \frac{S(\xi) [\sin(\overline{k_B \xi}) - \text{sign}(\overline{\eta}_0) |\overline{\eta}_0| S(\xi) \cos(\overline{k_B \xi})]}{1 + \overline{\eta}_0^2 S^2(\xi)} \right|. \quad (26)$$

Our derived solutions predict that the TDBS signal amplitude does not depend on the polarity (compression/tension) of the unipolar pulses and, as a consequence, it does not change even when the polarity changes to the opposite one upon reflection at a mechanically free surface. In contrast, for the anti-symmetric (odd) bipolar pulses incident on the SL structure, in the nonlinear regimes the Brillouin oscillation amplitude depends on the sign of the product of the sign of the strain leading phase (-/+ for compression/dilatation) and the sign of the exciton/phonon deformation potential. Thus, with the knowledge of the strain leading phase of the incident on the SL, the fitting of the Brillouin oscillation amplitude dependence on the pump laser power would provide opportunity to confirm the sign of the deformation potential, as it has been done in our experiments. This is a positive result of the developed theory.

Meanwhile, although in the strain pulse reflection from the mechanically free surface the polarities of both strain phases, i.e., of the leading and trailing parts, are inverted, the sequence of compression and tension phases in the sample coordinate system does not change after reflection. Thus, the sign of η_0 does not change after reflection of the bipolar strain pulse. Although the pulse propagates in the opposite direction after reflection, the left and the right phases of the reflected are of the same polarity as in the incident one. As in the developed theory the reflection on the mechanically free surface does not change $\text{sign}(\overline{\eta}_0)$ in odd bipolar pulses, it cannot be the reason for the experimentally observed difference in the oscillations amplitudes for the Stokes ($\nu > 0$) and anti-Stokes ($\nu < 0$) dependences. However, the above developed theory indicates that such difference could be expected when the profile of the strain pulse is asymmetric, i.e. neither odd nor even.

In general, i.e., nonlinear, regime the strain-induced profile of the permittivity variations $\Delta\varepsilon(z, t) \equiv \Delta\varepsilon(\eta(z, t))$ in Eq. (12) does not replicate the profile of the strain $\eta(z, t)$, although $\Delta\varepsilon(z, t)$ is a pulse propagating with the sound velocity. With increasing strain amplitude, the amplitude of the permittivity pulse, first, grows but later saturates, while its profile and length are continuously changing, following the continuous increase in the wings of the spatial strain profile due to the saturated core of $\Delta\varepsilon(z, t)$. In particular, continuous broadening of the permittivity pulse with the increase of strain amplitude is expected to manifest in continuous narrowing of $\Delta\varepsilon(z, t)$ spatial spectrum. As the TDBS signal amplitude is proportional to the amplitude of a particular fixed spatial spectrum component of the permittivity pulse (see Eq. (16)), the broadening of the permittivity pulses with strain leads to inevitable diminishing of the TDBS amplitude at sufficiently large strain. This explains qualitatively the non-monotonic dependences of the TDBS amplitude on the strain amplitude revealed in Eqs. (19) and (21) for the CPW with the profiles based on the Lorentzian function and the observation of the TDBS amplitude maximum in our experiments (Fig. 3 (a) of the main text).

The detailed theoretical analysis demonstrates that the deviations from the linear regime and the development of strongly nonlinear regime with increasing amplitude of the strain is expected to be very different for the strain of the same amplitude and duration, but different in their profiles. Particularly, the broadening of the permittivity pulses progresses with increasing strain amplitude significantly faster in the case of Lorentzian-based strain profiles than in the case of Gaussian-based ones, both for unipolar and bipolar strain pulses. For example, when the length of permittivity pulse under the action of the Lorentzian-based strain profile grows proportionally to power of strain, it could grow only logarithmically with strain under the action of the Gaussian-based strain profile. Thus, the significant qualitative differences between the theoretical predictions in Fig. 1 (a) of the Supplementary Material and the experimental

observations in Fig. 3 (a) in the main text can be mostly attributed to the Lorentzian-profile of the strain pulse used for the evaluation of the curves in Fig. 1 (a).

2. General description of photoelastic response for the real experimental parameters

While the adiabatic approximation explicitly illustrates the main features of the exciton photoelastic response and the main experimental observations, for numerical modeling we use a more general approach. The consideration is extended to the case of nonmonochromatic, i.e., arbitrary in duration, probe laser pulses and strain pulses also of an arbitrary duration, thus lifting adiabatic approximation. Moreover, the calculations are extended to the case of three-layer structure (air/active layer/substrate).

The electric field in the considered system can be obtained using Eqs. (1) and (2) in the spectral domain, i.e., by decomposing the light and strain pulses into their Fourier frequency components. It consists of the field, E_r , reflected from the surface of the sample and field, E_s , scattered on the strain pulse. Taking into account that intensity of light on a photodetector is proportional to EE^* , the transient reflectivity can be evaluated in the leading order, first, for the two-layer structure (air/semiconductor)

$$\frac{\Delta R}{R_0} = \frac{2 \int_{-\infty}^{\infty} dt \text{Re}\{E_s E_r^*\}}{\int_{-\infty}^{\infty} dt E_r E_r^*} = \frac{\Delta R_{2D} + \Delta R_{3D}}{R_0}, \quad (27)$$

where

$$dR_{2D} =$$

$$-\frac{2\omega_p}{\pi} \text{Re} \left\{ \int_{-\infty}^{\infty} d\omega \int_{-\infty}^{\infty} d\Omega k_0^3(\omega) \left(\frac{k_0(\omega) - k_1(\omega)}{k_0(\omega) + k_1(\omega)} \right)^* \frac{E_i^*(\omega) E_i(\omega - \Omega) e^{-i\Omega t_{pr}}}{(k_0(\omega) + k_1(\omega))(k_0(\omega) + k_1(\omega - \Omega))} \right. \\ \left. \times \left(\frac{\tilde{F}_-(\Omega)}{-(\omega - \Omega) + \omega_0 - i\Gamma} + \frac{\tilde{F}_+(\Omega)}{-\omega + \omega_0 - i\Gamma} \right) \left[\frac{1}{k_0(\omega) + k_1(\omega - \Omega) \mp \frac{\Omega}{v}} \right] \right\} \quad (28)$$

$$dR_{3D} =$$

$$\frac{\omega_p}{\pi^2} \text{Re} \left\{ \int_{-\infty}^{\infty} d\omega \int_{-\infty}^{\infty} d\Omega \int_{-\infty}^{\infty} d\Omega' k_0^3(\omega) \left(\frac{k_0(\omega) - k_1(\omega)}{k_0(\omega) + k_1(\omega)} \right)^* \frac{\tilde{E}_i^*(\omega) E_i(\omega - \Omega - \Omega') e^{-i(\Omega + \Omega') t_{pr}}}{(k_0(\omega) + k_1(\omega))(k_0(\omega) + k_1(\omega - \Omega - \Omega'))} \right. \\ \left. \times \frac{\tilde{F}_-(\Omega) \tilde{F}_+(\Omega')}{-(\omega - \Omega) + \omega_0 - i\Gamma} \left[\frac{1}{k_0(\omega) + k_1(\omega - \Omega - \Omega') \mp \frac{\Omega}{v}} \right] \right\}. \quad (29)$$

The solutions in Eqs. (28), (29) evidence the contribution to the transient reflectivity of all frequency components ω of the probe light pulses and all the modulation frequencies Ω introduced in the system by loading of the exciton polarization by dynamical strain. The wave vectors of light in vacuum and in SL are $k_0 = \frac{\omega}{c}$ and $k_1 = \frac{\omega}{c} \sqrt{\varepsilon_{\text{eff}}(\omega)}$, respectively, and $\varepsilon_{\text{eff}}(\omega)$ is described by Eq. (7). Parameter t_{pr} is the probe delay time. The functions \tilde{F}_{\pm} are the Fourier components of $F_{\pm}(t) = 2 \sin^2 \frac{\alpha_{\pm}(t)}{2} - i \sin \alpha_{\pm}(t)$, where $\alpha_{\pm}(t) = \pm \omega_d \int_{-\infty}^t dt' \eta(t')$. These functions describe the strain-induced shift/broadening of the exciton resonance: the larger strain amplitude - the wider frequency range with nonzero spectral components of \tilde{F}_{\pm} , which contribute to the denominators of the terms containing \tilde{F}_{\pm} in Eqs. (24) and (25).

The Fourier spectrum of the incident probe electric field reads

$$E_i(\omega) = \frac{\sqrt{\pi} \tau_l}{4} \exp(-i\psi_i) e^{-\left(\frac{\tau_l}{4}\right)^2 (\omega - \omega_i)^2}, \quad (30)$$

where τ_l is the full pulse duration at the $1/e^2$ level of the Gaussian probe pulse intensity, which is related to the full duration of the Gaussian probe pulse at the half of its maximal intensity, τ_{pr} , by relation $\tau_l = \sqrt{2/\ln 2} \tau_{pr}$.

In absence of strain the reflectivity reads

$$R_0 = \int_{-\infty}^{\infty} d\omega |E_i(\omega)|^2 \left| \frac{k_0(\omega) - k_1(\omega)}{k_0(\omega) + k_1(\omega)} \right|^2. \quad (31)$$

In the limit of small amplitude of strain, $\eta \rightarrow 0$, the term $dR_{3D} \rightarrow 0$. Thus, in the linear approximation the transient reflectivity can be simplified to:

$$\frac{\Delta R}{R_0} = \pm \frac{2\omega_p \omega_d}{\pi R} \text{Re} \left\{ \int_{-\infty}^{\infty} d\omega \int_{-\infty}^{\infty} d\Omega k_0^3(\omega) \left(\frac{k_0(\omega) - k_1(\omega)}{k_0(\omega) + k_1(\omega)} \right)^* \frac{\bar{E}_i^*(\omega) E_i(\omega - \Omega) e^{-i\Omega t_{pr}}}{(k_0(\omega) + k_1(\omega))(k_0(\omega) + k_1(\omega - \Omega))} \right. \\ \left. \times \frac{\tilde{\eta}(\Omega)}{(-(\omega - \Omega) + \omega_0 - i\Gamma)(-\omega + \omega_0 - i\Gamma)} \left[\frac{1}{k_0(\omega) + k_1(\omega - \Omega) \mp \frac{\Omega}{v}} \right] \right\} \quad (32)$$

The above formulas can be extended to the case of three-layer structure (air/SL/substrate), where SL of the thickness w is deposited on a semi-infinite substrate. In this case, the terms in square brackets in the expressions (32) should be replaced by

$$\frac{1}{\Delta_0(\omega)\Delta_0(\omega - \Omega)} \frac{1 - e^{iw(k_1(\omega) + k_1(\omega - \Omega) \mp \frac{\Omega}{v})}}{k_0(\omega) + k_1(\omega - \Omega) \mp \frac{\Omega}{v}} - r_{12}(\omega)r_{12}(\omega - \Omega) \frac{1 - e^{iw(k_1(\omega) + k_1(\omega - \Omega) \pm \frac{\Omega}{v})}}{k_0(\omega) + k_1(\omega - \Omega) \pm \frac{\Omega}{v}} e^{2iw(k_2(\omega) + k_2(\omega - \Omega))}, \quad (33)$$

where $\Delta_0 = r_{10}r_{12}e^{2iwk_2}$, k_2 is the wavevector of light in the substrate and r_{12} is the reflectivity coefficient at the interface SL/substrate. Similarly, in the general regime of nonlinear photo-elasticity the solutions for the case of finite width SL can be obtained by modification of the terms in the square brackets in Eqs. (28) and (29). In the solution for dR_{2D} the term in the square brackets should be replaced by Eq. (33), while in the solution for dR_{3D} by a modified Eq. (33), where $\omega - \Omega$ is shifted to $\omega - \Omega - \Omega'$ and $\frac{\Omega}{v}$ to $\frac{\Omega + \Omega'}{v}$.

Eqs. (27) - (33) was applied for the evaluation of the results presented in Fig. 2(b), (c) and Fig. 3(a), (c) of the main text, via modeling of the strain profile by the derivative of the Gaussian with duration between minimum and maximum of the profile, $\tau_a = 12.5$ ps. The following parameters were used for calculations: $\Xi = -10$ eV, $\Gamma = 0.7$ meV, $\omega_{LT} = 0.13$ meV, $\tau_L = 2.29$ ps, and $v = 5105$ m/s. A good agreement between experimental results and calculations is reached. The agreement can be improved by using even more realistic profile of the strain pulse, however, this is beyond our current scopes.

References

1. A. N. Poddubny, A. V. Poshakinskiy, B. Jusserand, and A. Lemaitre. Phys. Rev. B **89**, 235313 (2014).
2. C. Thomsen, H. T. Grahn, H. J. Maris, and J. Tauc, Phys. Rev. B, **34**, 4129 (1986).
3. V. Gusev, Acustica **82**, S-37 (1996).
4. B. Jusserand, A. N. Poddubny, A. V. Poshakinskiy, A. Fainstein, and A. Lemaitre, Phys. Rev. Lett. **115**, 267402 (2015).
5. O. B. Wright, B. Perrin, O. Matsuda, and V. E. Gusev, Phys. Rev. B **64**, 081202 (2001).